



RESEARCH LETTER

10.1002/2017GL074509

Key Points:

- The majority of CMIP5 models project robust increases in the spatial extent of ENSO temperature and precipitation teleconnections over land
- The increase in area is related to the amplified ENSO-driven precipitation across the equatorial Pacific in the future
- Despite the robust increase in area over land, we do not find a consistent strengthening of these teleconnections in the individual models

Supporting Information:

- Supporting Information S1

Correspondence to:

S. J. Perry,
s.perry@student.unsw.edu.au

Citation:

Perry, S. J., McGregor, S., Gupta, A. S., & England, M. H. (2017). Future changes to El Niño–Southern Oscillation temperature and precipitation teleconnections. *Geophysical Research Letters*, 44, 10,608–10,616. <https://doi.org/10.1002/2017GL074509>

Received 16 JUN 2017

Accepted 4 OCT 2017

Accepted article online 9 OCT 2017

Published online 21 OCT 2017

Future Changes to El Niño–Southern Oscillation Temperature and Precipitation Teleconnections

Sarah J. Perry^{1,2,3} , Shayne McGregor^{2,3} , Alex Sen Gupta^{1,3} , and Matthew H. England^{1,3} 

¹Climate Change Research Centre, University of New South Wales, Sydney, New South Wales, Australia, ²School of Earth, Atmosphere and Environment, Monash University, Melbourne, Victoria, Australia, ³Australian Research Council Centre of Excellence for Climate System Science, University of New South Wales, Sydney, New South Wales, Australia

Abstract Potential changes to the El Niño–Southern Oscillation (ENSO) resulting from climate change may have far reaching impacts through atmospheric teleconnections. Here ENSO temperature and precipitation teleconnections between the historical and high-emission future simulations are compared in 40 models from phase 5 of the Coupled Model Intercomparison Project. Focusing on the global land area only, we show that there are robust increases in the spatial extent of ENSO teleconnections during austral summer in 2040–2089 of ~19% for temperature and ~12% for precipitation in the multimodel mean (MMM), relative to the 1950–1999 period. The MMM further shows that the expansion of ENSO teleconnection extent is at least partly related to a strengthening of ENSO teleconnections over continental regions; however, a consistent strengthening is not found across the individual models. This suggests that while more land may be affected by ENSO, the existing teleconnections may not be simply strengthened.

1. Introduction

The El Niño–Southern Oscillation (ENSO) is the largest source of interannual climate variability, contributing to substantial changes in rainfall, temperature, and extreme weather around the globe. Although there are robust projections of climate change impacts for changes in the long-term average temperature and precipitation for the next century (Intergovernmental Panel on Climate Change, 2014), there remains uncertainty around how the characteristics of ENSO and its teleconnections may change in the future (Collins et al., 2010), despite models showing an increase in the frequency of extreme ENSO events (Cai et al., 2015). The uncertainty arises from the different representations of the coupled ocean and atmosphere feedback processes that control ENSO, with models from phase 5 of the Coupled Model Intercomparison Project (CMIP5) showing no clear consensus on whether ENSO sea surface temperature (SST) variability will increase or decrease (Guilyardi et al., 2009; Stevenson et al., 2012; Watanabe et al., 2012).

Despite the lack of agreement in projected changes to ENSO SST variability, recent studies have shown that there is a consistent projected strengthening of the atmospheric response to ENSO across the equatorial Pacific. Power et al. (2013) show that for ENSO SST anomalies (SSTAs) of the same structure and magnitude, anomalous convection is greater in the 21st century compared to the 20th century due to background warming in the equatorial Pacific. They further show that the nonlinear contribution to intensified precipitation from background warming can be enhanced or damped by projected changes in ENSO variance and structural changes to ENSO SSTAs, which have less intermodel agreement. Cai et al. (2014) also show that the faster rates of warming projected for the equatorial and eastern Pacific reduce the zonal and meridional gradients of SST, increasing the frequency of deep convection anomalies including the southward shift of the intertropical convergence zone that signifies extreme El Niño events.

The enhanced thermodynamic response in the central and eastern Pacific is the result of the interaction between the warmer and moister atmosphere (Held & Soden, 2006; Huang & Xie, 2015) and the total SST arising from ENSO SSTAs superimposed upon the mean warming of the equatorial Pacific (Johnson & Xie, 2010), forming conditions that are more conducive to deep convection and contributing to an eastward shift of the convective heating anomaly (Cai et al., 2014; Power et al., 2013). As the latent heat release from anomalous deep convection is the driving mechanism of atmospheric teleconnections that cause the remote impacts of ENSO (Chiang & Sobel, 2002; Hoskins & Karoly, 1981; Trenberth et al., 1998), it follows that increases in ENSO-driven convection in the tropical Pacific may cause changes in ENSO teleconnections to remote regions (Watanabe et al., 2014).

Recent model studies have begun to provide insight into potential changes to ENSO teleconnections. Using atmosphere-only models, Zhou et al. (2014) show that the eastward shift of deep convection during El Niño combined with mean warming drives a strengthened Pacific North America teleconnection pattern, intensifying the ENSO-driven precipitation variability across North America. This is also consistent with other studies that suggest geographical changes in ENSO teleconnections, the magnitude of which depend on both external forcing and ENSO amplitude changes (e.g., Kug et al., 2010; Meehl & Teng, 2007; Stevenson, 2012). For example, in a global study, Bonfils et al. (2015) project the observed pattern of ENSO variability onto CMIP5 model output from the historical and RCP8.5 simulations to obtain a “typical” ENSO SST pattern and associated precipitation teleconnections for the current and future climates. They find intensified ENSO-driven precipitation in the future simulations and show that this increase in precipitation response is modulated by the projected change in the amplitude of ENSO variability in each model (Bonfils et al., 2015). To date, there has been limited research investigating future changes in temperature teleconnections or examining in detail changes over land where ENSO events have the greatest societal impacts. Here we expand upon the analysis of Power et al. (2013) by examining a larger ensemble of CMIP5 models and broadening the focus from the equatorial Pacific Ocean to identify the changes in ENSO-driven variability that occur over remote land areas.

2. Methods

2.1. Data

We analyze monthly precipitation and surface temperature output from 40 CMIP5 models (see Taylor et al., 2012; supporting information Table S1). We compare the ENSO teleconnections simulated in different climate conditions over two 50 year periods: between 1950 and 1999 in the historical simulations and between 2040 and 2089 in the high-emission RCP8.5 simulations, where anthropogenic radiative forcing reaches 8.5 W m^{-2} by 2100. For models that have archived multiple historical and RCP8.5 simulations, we use output from the first ensemble member only. The data processing and identification of the ENSO signal follows Power et al. (2013). Surface temperature and precipitation data are interpolated to a 1.5° latitude by 1.5° longitude grid, and a high-pass spectral filter is applied to remove variability with a period greater than 13 years including the climatological mean, global warming signal, and any multidecadal variability. Subsequent analysis focuses on the austral summer season, December-January-February (DJF), when ENSO variability peaks. For comparison with observed ENSO teleconnections, we analyze observations of temperature from the National Centers for Environmental Prediction (NCEP)/National Center for Atmospheric Research (NCAR) reanalysis (Kalnay et al., 1996) for a comparable 50 year period between 1953 and 2002 and precipitation from the CPC Merged Analysis of Precipitation (CMAP) data set (Xie & Arkin, 1997) between 1984 and 2010, applying the same temporal filtering outlined above. The first and last 5 years of the data sets are discarded to minimize edge effects introduced by the spectral filter.

2.2. Identifying ENSO and ENSO Teleconnections

Following Power et al. (2013), ENSO patterns for models and observations were calculated using an empirical orthogonal function (EOF) analysis of the equatorial ocean domain (30°S – 30°N , 0 – 360°E). The first EOF of both the equatorial ocean SST and precipitation represents the ENSO mode, with its associated principle component (PC) illustrating the temporal evolution of El Niño and La Niña events. Separate EOFs were calculated for each model for each 50 year time period, and for both SST and precipitation, to identify if structural changes in ENSO or ENSO's teleconnections are apparent. The first PCs for temperature and precipitation are highly correlated for each model with an ensemble median correlation of 0.94 (interquartile range (IQR) of 0.91–0.97) for the historical period. The ENSO signal is insensitive to the zonal domain: the correlation between the first PC for the equatorial ocean and the equatorial Pacific Ocean exceeds 0.98 for the majority of models.

To identify global ENSO teleconnection patterns, the normalized SST and precipitation PCs were linearly regressed against the respective global surface temperature or precipitation filtered time series at all locations. The resulting regression maps (Figure 1) illustrates the mean change in temperature or precipitation (in degrees Celsius or millimeters per day) at each grid point that is associated with a one standard deviation change in the ENSO PC. The strongest relationships are expected over the equatorial Pacific Ocean, the source of ENSO variability, with significant ($p < 0.05$) regressions elsewhere indicative of remote ENSO teleconnections. The proportion of global land area having a significant regression is

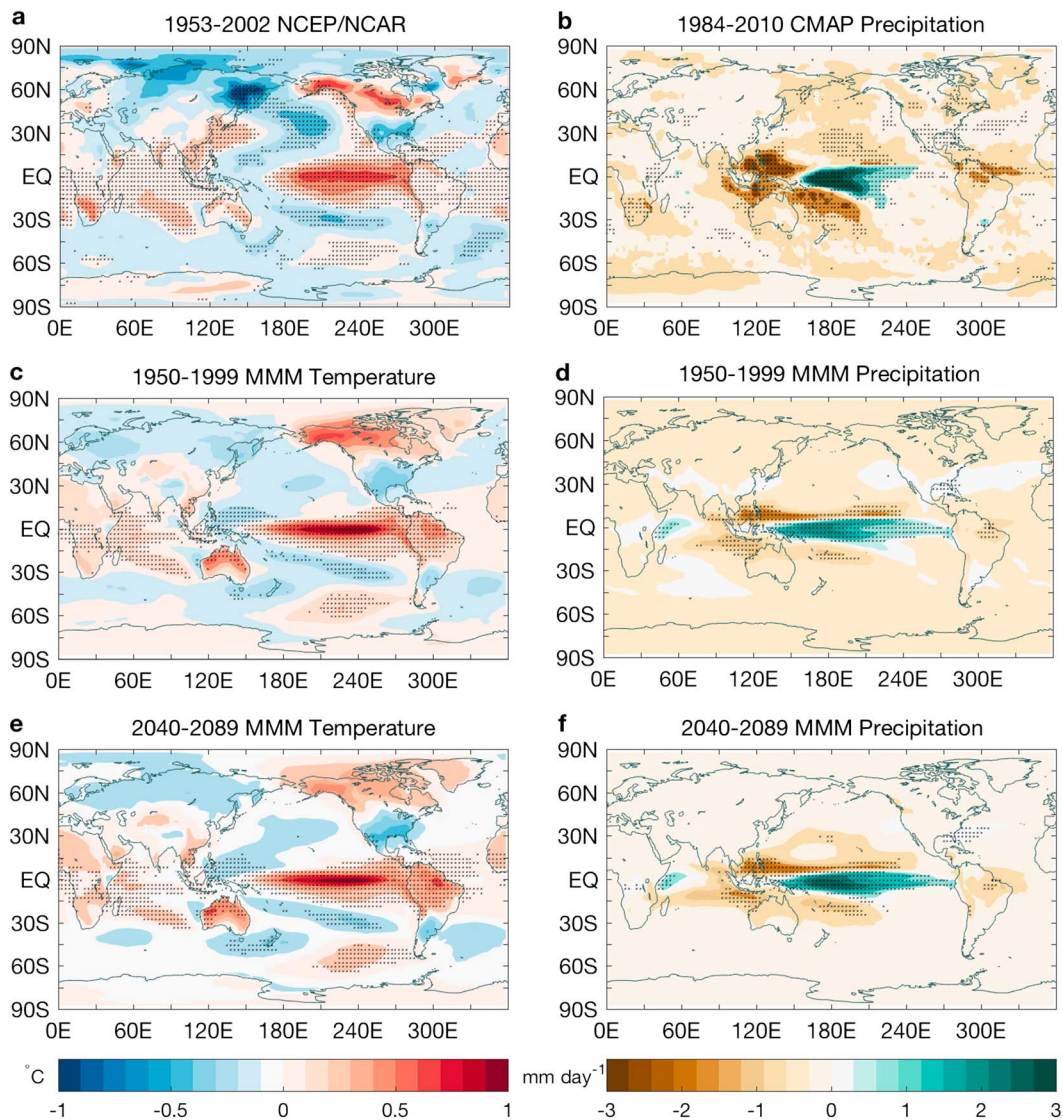


Figure 1. Regression of normalized ENSO index (defined in section 2.2) on global surface temperature and precipitation. (a) NCEP/NCAR reanalysis temperature observations (1953–2002), (b) CMAP precipitation observations (1984–2010), (c and d) MMM historical simulations (1950–1999), (e and f) MMM RCP8.5 simulations (2040–2089). Stippling in Figures 1a and 1b shows significant regressions at $p < 0.05$. Stippling in Figures 1c–1f shows significant teleconnections in the MMM (where 25 out of 40 models agree on the location of significant teleconnections, corresponding to a significance level of $p < 0.1$).

hereafter referred to as the spatial extent of the ENSO teleconnections. We further test where there is agreement across the model ensemble in the location of significant ENSO teleconnections. When at least 25 out of the 40 models show a statistically significant regression with ENSO at a given location the level of intermodel agreement (62.5%) is considered significant at $p < 0.1$ based on a binomial distribution (Power et al., 2012), assuming that each model is an independent sample (Annan & Hargreaves, 2017). Regions that meet this requirement for intermodel agreement are hereafter referred to as having a significant MMM teleconnection.

3. Results

3.1. Comparison to Observed ENSO Teleconnections

Previous studies have shown that the CMIP5 models are capable of simulating the dynamics of ENSO with varying degrees of fidelity (e.g., Bellenger et al., 2014; Taschetto et al., 2014; Weare, 2013). Comparison of the multimodel mean (MMM) teleconnection maps from the historical period with the observed

teleconnection maps (Figure 1) indicates that the MMM captures the broadscale observed ENSO teleconnections. The spatial correlation between the MMM temperature teleconnection for the historical period and the observed teleconnection for all land areas is 0.61. Significant ($p < 0.05$) observed temperature teleconnections cover 36.2% of the global land area (stippling in Figure 1a). This is within the range of the individual CMIP5 models and is similar to the median spatial extent of 37.0% (IQR of 30.2–47.0%) (supporting information Table S1). However, only 17.4% of the global land area has a significant MMM teleconnection (where at least 25 out of 40 models agree, corresponding to $p < 0.1$). This area is shown by the stippling in Figure 1c and includes parts of northern South America, Central Africa, the Maritime Continent, and northern Australia. Despite the broad similarity of the observed and MMM teleconnection, the spatial correlation between the observed and simulated temperature teleconnections over land in the individual models is relatively low, with an ensemble median of 0.34 (IQR of 0.22–0.50).

The spatial correlation between the MMM precipitation teleconnection map for the historical period and the observed teleconnection map for the global land area is 0.56. This is again considerably higher than the spatial correlation between the observed and simulated precipitation teleconnections over land for most individual models, which have a median correlation of 0.38 (IQR of 0.30–0.44). The spatial extent of the observed precipitation teleconnection is smaller than the temperature teleconnection, covering 23.5% of the global land area (stippling in Figure 1b). This observed area of significant teleconnections over land falls in the lower range of the individual model spread, where the median percentage of land with a significant precipitation teleconnection is 26.4% (IQR of 18.9–32.7%) (supporting information Table S1). As with temperature, the models show limited agreement in the locations where ENSO teleconnections are significant, with a significant MMM teleconnection covering only 3.12% of the global land area for precipitation (stippling in Figure 1d).

For both temperature and precipitation, the limited intermodel agreement in the MMM teleconnections and the low spatial correlation when compared to the observed teleconnections are influenced by: (i) the differences in the individual models representation of ENSO SSTAs and subsequently its teleconnections (Bellenger et al., 2013; Taschetto et al., 2014; Weare, 2013), and (ii) stochastic noise arising from the use of relatively short 50 year time periods to derive the ENSO teleconnections (Batehup et al., 2015; Wittenberg, 2009). The effect of the short record is further discussed in section 3.2.

3.2. Global Changes to ENSO Teleconnections

We now focus on how ENSO teleconnections over land are projected to change subject to continued high emissions as per the RCP8.5 simulations. The spatial similarities between the 1950–1999 and 2040–2089 periods are clear from the MMM teleconnection maps (Figures 1c–1f), as reflected by the spatial correlation over land of 0.95 for both temperature and precipitation. Despite the similarity of the MMM patterns, the median spatial correlation for the global land area across the models between the two periods is 0.44 (IQR of 0.32–0.67) for temperature and 0.69 (IQR of 0.54–0.80) for precipitation. To examine if the projected changes in the teleconnection patterns are a result of external forcing or internal variability, we compare the spatial correlations of DJF ENSO teleconnection maps for an ensemble of simulations from two models: HadGem2-ES and CCSM4 (supporting information Tables S2 and S3). We seek to determine if the range of spatial correlations over land between the historical and future simulations in these models lies outside the range of stochastic variability sampled between model ensemble members during the historical period. To this end, a two-sample t test was calculated between the two distributions (historical-historical versus historical-future) for each model and for temperature and precipitation. Three of the four comparisons revealed correlations between the historical and future teleconnections that were not statistically different ($p < 0.05$) from comparison within the historical period itself. This suggests that the stochasticity of the climate system is likely to have a strong influence on the low spatial correlation in individual ensemble members, and as such it will be hard to separate from any forced signal.

To further examine whether changes are occurring in ENSO teleconnections over land, we calculate the change in area of significant teleconnections between the two time periods. Examining the models individually, we find that the land area with significant ENSO temperature teleconnections increases in 28 out of 40 models (Figure 2a and supporting information Table S1). This level of model agreement is significant above the 99% level ($p < 0.01$) based on a binomial distribution. For the individual models, the mean change in spatial extent is 10.15% (IQR of –5.68 to 26.6%) (supporting information Table S1), relative to the

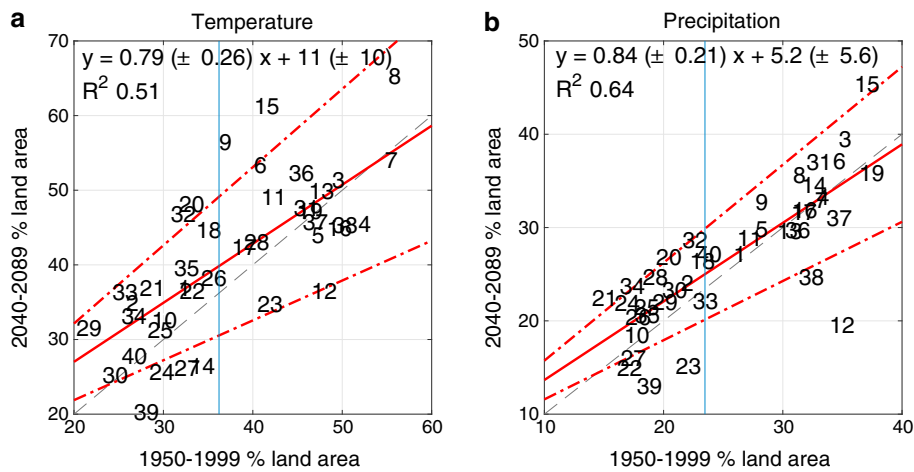


Figure 2. Percentage of the global land area that has a significant regression with ENSO ($p < 0.05$) for the historical and future periods in each model for (a) temperature and (b) precipitation. The relationship between the two time periods for the ensemble is given by the regression equation y (solid red line) including the upper and lower 95% confidence intervals for the slope (dashed red lines). Reference numbers correspond to models given in supporting information Table S1. The blue line indicates the percentage of land with a significant ENSO teleconnection in the observations. The grey dashed line illustrates the 1:1 line.

1950–1999 period, and is significantly different from 0 ($p < 0.05$) using a t test. The land area with a significant MMM teleconnection (where at least 25 out of 40 models agree, corresponding to $p < 0.1$) increases by approximately 19% in the 2040–2089 period, relative to the 1950–1999 period. This is most prominent over equatorial Africa, South America, and Australia (Figures 1c and 1e).

For precipitation, the land area with a significant precipitation teleconnection is also increasing in 27 out of 40 models (Figure 2b and supporting information Table S1), with an equivalent significance level of $p < 0.02$ based on a binomial distribution. The mean change over land in the individual models, relative to the 1950–1999 period, is 5.93% (IQR of -3.70 to 14.5%) (supporting information Table S1); however, this change is not significant ($p < 0.05$) using a t test. The area with a significant precipitation teleconnection in the MMM similarly shows an increase in the future period, although the change is smaller than that found for temperature. The increase in the land area with a significant MMM teleconnection is approximately 12% relative to the 1950–1999 period and primarily occurs over equatorial Africa and South America, including an area over northern Chile that is significant in the future period only (Figures 1d and 1f).

To determine if this change in ENSO teleconnections is seasonally dependent, we repeat our analysis for the other seasons (March–April–May, June–July–August, and September–October–November) and for an annual average calculated between July and June of the following year. The spatial extent of significant teleconnections in the MMM and individual models differs with the seasons for both temperature and precipitation (supporting information Figure S1). However, the spatial extent of significant temperature teleconnections over land for the individual models is increasing for all seasons and the annual average. The level of intermodel agreement for the increase in area is significant above the 90% level ($p < 0.1$) in all cases (supporting information Figure S1). In contrast, the precipitation teleconnection is found to have significant intermodel agreement ($p < 0.02$) on the increase in the area of significant teleconnections over land for DJF only (supporting information Figure S1). For the annual average and all other seasons there is no significant agreement across the ensemble in the change in teleconnections over land for precipitation.

3.3. Relationship to Changes in ENSO Variance

We next examine whether the projected change in teleconnection spatial extent is dependent on the change in ENSO variability to determine if those models with enhanced (suppressed) ENSO variability in the future simulations also have increased (decreased) ENSO teleconnections. We compare the change in area of significant ENSO teleconnections to the change in standard deviation of the SSTa in the Niño 3.4 region (190°E – 240°E , 5°S – 5°N), calculated using high-pass filtered DJF means for each model. The change in standard deviation between the two time periods was normalized by the historical standard deviation for each model to illustrate the proportional change in variability relative to the models initial ENSO variability. Figures 3a and 3b show that there is a significant ($p < 0.05$) intermodel relationship between the change in ENSO variability

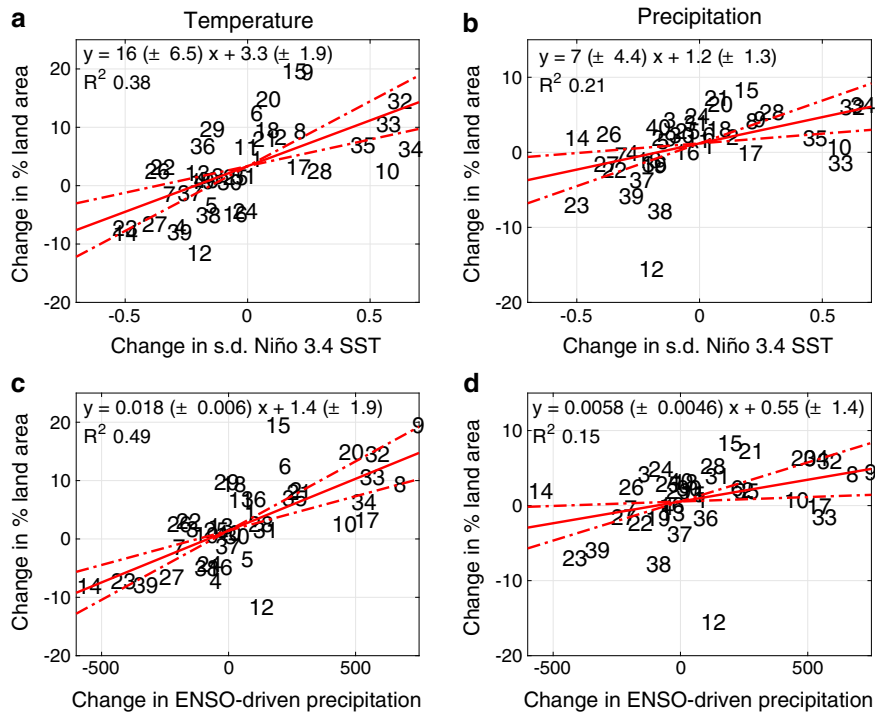


Figure 3. The relationship between the change in teleconnection spatial extent over land versus the change in ENSO variability. (a and b) ENSO variability is the change in standard deviation of the Niño3.4 region SSTAs, (c and d) the change in the total sum of the precipitation regression coefficients over the tropical Pacific Ocean (120–290°E, 10°S–10°N). The regression relationship for the ensemble is shown by equation y (solid red lines) including the upper and lower 95% confidence intervals for the slope (dashed red lines). Reference numbers correspond to models given in supporting information Table S1.

and the change in the area of significant ENSO teleconnections during DJF for both temperature and precipitation, suggesting that part of the change in teleconnection area can be associated with changes in ENSO variability in the future. For example, each model with enhanced ENSO variability also shows an increase in the temperature teleconnection spatial extent, but not all the models with reduced ENSO variability show decreases in spatial extent. This contributes to the positive offset of the regression model, which suggests that models displaying no change in ENSO variability will on average display an increase in the spatial extent of significant temperature teleconnections over land. A similar relationship is also evident for the precipitation teleconnection; however, there are a few models with increased ENSO SSTA variability that also show decreasing teleconnection spatial extent (Figure 3b). Thus, the positive offsets of the regression models (Figures 3a and 3b) suggest an increase in the teleconnection area that is unrelated to the changes in ENSO SSTA variability.

As previous studies have shown that the precipitation response in the tropics to unchanged ENSO SSTAs is enhanced in future climate conditions (Chung et al., 2014; Power et al., 2013), we further compare the change in teleconnection area to the change in the total ENSO-driven precipitation over the equatorial Pacific Ocean. We define the change in ENSO-driven precipitation as the difference between the cumulative sum of precipitation regression coefficients over the equatorial Pacific Ocean between 120–290°E and 10°S–10°N (cf. Figures 1d and 1f). A significant ($p < 0.05$) intermodel relationship is found for the change in ENSO-driven precipitation and teleconnection area for both temperature and precipitation (Figures 3c and 3d). For temperature, the majority of models show increased (decreased) teleconnections associated with increased (decreased) ENSO-driven precipitation, with the change in ENSO-driven precipitation explaining a greater portion of the change in teleconnection area than the change in ENSO SSTA variance. Further, the positive offset is reduced, suggesting that the increased ENSO-driven precipitation response is at least partly responsible for the increased ENSO temperature teleconnections over land. However, the result is not clear for precipitation; although the positive offset is again slightly reduced, ENSO SSTA variance explains more of the change in precipitation teleconnections than the change in precipitation over the equatorial Pacific Ocean.

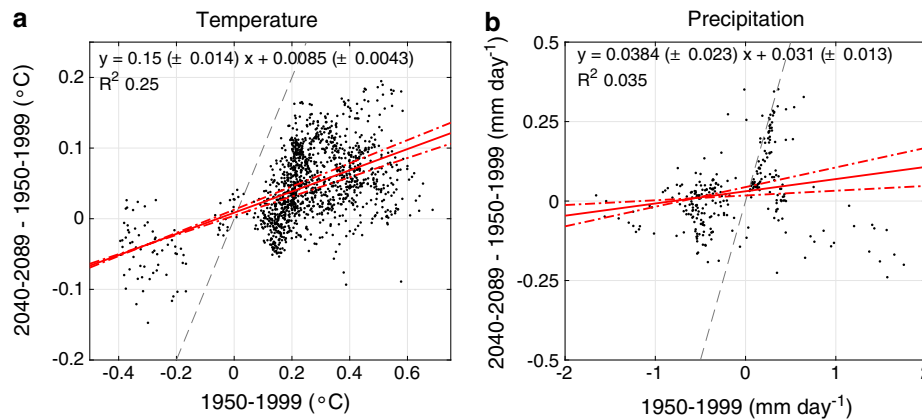


Figure 4. The relationship between the change in teleconnections (future-historical MMM regression coefficients) and the historical teleconnections for land areas where there is a significant teleconnection in the MMM (where 25 out of 40 models agree on the location of significant teleconnections, corresponding to a significance level of $p < 0.1$), for (a) temperature and (b) precipitation. Each point represents a land grid point that is significant in the MMM in one or both time periods. The regression relationship is given by the equation y (solid red lines) including the upper and lower 95% confidence intervals on the slope (dashed red lines). The grey dashed line illustrates the 1:1 line.

3.4. Changes to the Strength of the ENSO Teleconnections Over Land

Here we examine whether the intensity of the ENSO teleconnections over land during DJF is also strengthened in the future period. Comparison of the MMM difference between the historical and future teleconnection maps (supporting information Figure S2) indicates that there are regions where the strength of ENSO's teleconnections, calculated as the magnitude of the regression coefficients, is projected to change. A two-sided t test was calculated to determine if the mean of the regression coefficients for the individual models at each grid point is significantly different ($p < 0.05$) between the historical and future simulations (stippling in supporting information Figure S2). Based on regions that have a significant teleconnection in the MMM in either period, increases in the temperature teleconnection strength are evident over areas of South America, eastern, and western Africa. Changes in the strength of the precipitation teleconnection are evident for central and eastern Africa (supporting information Figure S2).

We quantify the magnitude of the change in teleconnection strength over land by comparing the difference between the regression coefficients (2040–2089 to 1950–1999) at the locations where there is a significant teleconnection in the MMM in either period (stippling in Figures 1c–1f) against the historical period (Figure 4). The regression slope (0.15 ± 0.014) indicates that the MMM temperature teleconnection at these locations is on average stronger in the future period (Figure 4a). However, the relatively low R^2 of 0.25 suggests that this strengthening is not a uniform intensification of the historical MMM temperature teleconnection over land (cf. supporting information Figure S3a). This is also the case for the MMM precipitation teleconnection (Figure 4b), which displays a slight strengthening in the future period (0.04 ± 0.023), while the low R^2 of 0.03 indicates little similarity between the teleconnection change and the historical teleconnection (cf. supporting information Figure S3b). Comparing the change in teleconnection strength for the same land area as the MMM in the individual models also reveals there is no significant intermodel agreement (based on the binomial distribution) on a strengthening of the teleconnections over land (supporting information Figure S4). This is at least partly influenced by noise in the climate system, which is reduced in the MMM, as discussed in section 3.2. However, we do find a clear relationship between the change in each models ENSO teleconnection strength and the change in the teleconnection spatial extent over land, with larger changes in teleconnection area associated with strengthened teleconnections (supporting information Figure S4).

4. Summary and Conclusion

Recent studies have shown a consistent projected strengthening of the atmospheric response to ENSO SSTAs across the equatorial Pacific (Cai et al., 2014; Power et al., 2013), which may enhance remote teleconnections due to the increase in latent heating (Watanabe et al., 2014). Our analysis shows that with future warming under the RCP8.5 simulations, the spatial extent of ENSO temperature teleconnections in the MMM (where

at least 25 out of 40 models agree on the location of teleconnections, corresponding to $p < 0.1$) increases by approximately 19% in the 2040–2089 period relative to 1950–1999, and this increase is seen regardless of the season analyzed. The MMM precipitation teleconnection increases in area by approximately 12%; however, a significant change only occurs during DJF. Although there is spread across the individual ensemble members regarding the change in teleconnection area, we find a significant level of agreement for an increase in area amongst the individual models that is also robust when separating the models according to the teleconnection skill (supporting information Table S1). This may have implications for reconstructions of past ENSO variability from remote proxies that assume ENSO teleconnections are stationary (Li et al., 2011, 2013; McGregor et al., 2013, 2010).

In agreement with previous studies (Bonfils et al., 2015), we show that changes in the spatial extent of the ENSO teleconnections are at least partly related to the change in amplitude of SSTAs in the Niño 3.4 region. However, the amplitude changes cannot entirely explain the mean increase in the spatial extent of ENSO teleconnections over land. This is supported by the fact that approximately half of all models displaying reduced future ENSO amplitudes display an increase in the teleconnection spatial extent. We further show there is a relationship between this mean change in area and ENSO-driven precipitation across the equatorial Pacific, consistent with the suggestions of Power et al. (2013), Cai et al. (2014), and Watanabe et al. (2014). It is important to note that neither predictor explains more than half of the intermodel differences in the change in spatial extent, suggesting there may be additional mechanisms that contribute to this change in teleconnection area that have not yet been considered. Further exploration of the underlying mechanisms remains an avenue for future work.

For land areas where there are significant MMM teleconnections, we show that although the MMM teleconnection is strengthened in the future period this strengthening varies by location for both temperature and precipitation. Further, analysis of the individual models does not show a consistent strengthening of the teleconnection over land. As the strengthening of the future teleconnection over land areas lacks consistency across the individual models, we suggest that while the land area that is being impacted by ENSO variability is increasing, it is unlikely that the future teleconnections will simply reflect an enhancement of the historical teleconnections.

Acknowledgments

We acknowledge the World Climate Research Programme's Working Group on Coupled Modeling and the climate modeling groups listed in supporting information Table S1 for producing and making available CMIP5 model output. This research was supported by the Australian Research Council (ARC) including the ARC Centre of Excellence in Climate System Science. We would also like to thank the two reviewers for their constructive feedback.

References

- Annan, J. D., & Hargreaves, J. C. (2017). On the meaning of independence in climate science. *Earth System Dynamics*, 8(1), 211–224. <https://doi.org/10.5194/esd-8-211-2017>
- Batehup, R., McGregor, S., & Gallant, A. J. E. (2015). The influence of non-stationary teleconnections on palaeoclimate reconstructions of ENSO variance using a pseudoproxy framework. *Climate of the Past*, 11(12), 1733–1749. <https://doi.org/10.5194/cp-11-1733-2015>
- Bellenger, H., Guilyardi, E., Leloup, J., Lengaigne, M., & Vialard, J. (2014). ENSO representation in climate models: From CMIP3 to CMIP5. *Climate Dynamics*, 42(7–8), 1999–2018. <https://doi.org/10.1007/s00382-013-1783-z>
- Bonfils, C. J. W., Santer, B. D., Phillips, T. J., Marvel, K., Ruby Leung, L., Doutriaux, C., & Capotondi, A. (2015). Relative contributions of mean-state shifts and ENSO-driven variability to precipitation changes in a warming climate. *Journal of Climate*, 28(24), 9997–10,013. <https://doi.org/10.1175/JCLI-D-15-0341.1>
- Cai, W., Borlace, S., Lengaigne, M., van Rensch, P., Collins, M., Vecchi, G., ... Jin, F. F. (2014). Increasing frequency of extreme El Niño events due to greenhouse warming. *Nature Climate Change*, 4(2), 111–116. <https://doi.org/10.1038/nclimate2100>
- Cai, W., Santoso, A., Wang, G., Yeh, S. W., An, S. I., Cobb, K. M., ... Wu, L. (2015). ENSO and greenhouse warming. *Nature Climate Change*, 5(9), 849–859. <https://doi.org/10.1038/nclimate2743>
- Chiang, J. C. H., & Sobel, A. H. (2002). Tropical tropospheric temperature variations caused by ENSO and their influence on the remote tropical climate. *Journal of Climate*, 15(18), 2616–2631. [https://doi.org/10.1175/1520-0442\(2002\)015%3C2616:TTVCB%3E2.0.CO;2](https://doi.org/10.1175/1520-0442(2002)015%3C2616:TTVCB%3E2.0.CO;2)
- Chung, C. T. Y., Power, S. B., Arblaster, J. M., Rashid, H. A., & Roff, G. L. (2014). Nonlinear precipitation response to El Niño and global warming in the Indo-Pacific. *Climate Dynamics*, 42(7–8), 1837–1856. <https://doi.org/10.1007/s00382-013-1892-8>
- Collins, M., An, S. I., Cai, W., Ganachaud, A., Guilyardi, E., Jin, F. F., ... Wittenberg, A. (2010). The impact of global warming on the tropical Pacific ocean and El Niño. *Nature Geoscience*, 3(6), 391–397. <https://doi.org/10.1038/ngeo868>
- Guilyardi, E., Wittenberg, A., Fedorov, A., Collins, M., Wang, C., Capotondi, A., ... Stockdale, T. (2009). Understanding El Niño in ocean-atmosphere general circulation models: Progress and challenges. *Bulletin of the American Meteorological Society*, 90(3), 325–340. <https://doi.org/10.1175/2008BAMS2387.1>
- Held, I. M., & Soden, B. J. (2006). Robust responses of the hydrologic cycle to global warming. *Journal of Climate*, 19(21), 5686–5699. <https://doi.org/10.1175/JCLI3990.1>
- Hoskins, B. J., & Karoly, D. J. (1981). The steady linear response of a spherical atmosphere to thermal and orographic forcing. *Journal of the Atmospheric Sciences*, 38(6), 1179–1196. [https://doi.org/10.1175/1520-0469\(1981\)038%3C1179:TSLROA%3E2.0.CO;2](https://doi.org/10.1175/1520-0469(1981)038%3C1179:TSLROA%3E2.0.CO;2)
- Huang, P., & Xie, S.-P. (2015). Mechanisms of change in ENSO-induced tropical Pacific rainfall variability in a warming climate. *Nature Geoscience*, 8(12), 922–926. <https://doi.org/10.1038/ngeo2571>
- Intergovernmental Panel on Climate Change (2014). In Core writing team, R. K. Pachauri, & L. A. Meyer (Eds.), *Climate change 2014: Synthesis report. Contribution of Working Groups I, II and III to the Fifth Assessment Report of the Intergovernmental Panel on Climate Change* (p. 151). Geneva, Switzerland: IPCC.

- Johnson, N. C., & Xie, S. P. (2010). Changes in the sea surface temperature threshold for tropical convection. *Nature Geoscience*, 3(12), 842–845. <https://doi.org/10.1038/Ngeo1008>
- Kalnay, E., Kanamitsu, M., Kistler, R., Collins, W., Deaven, D., Gandin, L., ... Joseph, D. (1996). The NCEP/NCAR 40-year reanalysis project. *Bulletin of the American Meteorological Society*, 77(3), 437–471. [https://doi.org/10.1175/1520-0477\(1996\)077%3C0437:TNYRP%3E2.0.CO;2](https://doi.org/10.1175/1520-0477(1996)077%3C0437:TNYRP%3E2.0.CO;2)
- Kug, J. S., Il An, S., Ham, Y. G., & Kang, I. S. (2010). Changes in El Niño and La Niña teleconnections over North Pacific-America in the global warming simulations. *Theoretical and Applied Climatology*, 100(3–4), 275–282. <https://doi.org/10.1007/s00704-009-0183-0>
- Li, J., Xie, S.-P., Cook, E. R., Huang, G., D'Arrigo, R., Liu, F., ... Zheng, X.-T. (2011). Interdecadal modulation of El Niño amplitude during the past millennium. *Nature Climate Change*, 1(2), 114–118. <https://doi.org/10.1038/nclimate1086>
- Li, J., Xie, S. P., Cook, E. R., Morales, M. S., Christie, D. A., Johnson, N. C., ... Fang, K. (2013). El Niño modulations over the past seven centuries. *Nature Climate Change*, 3(9), 822–826. <https://doi.org/10.1038/nclimate1936>
- McGregor, S., Timmermann, A., England, M. H., Elison Timm, O., & Wittenberg, A. T. (2013). Inferred changes in El Niño–Southern Oscillation variance over the past six centuries. *Climate of the Past*, 9(5), 2269–2284. <https://doi.org/10.5194/cp-9-2269-2013>
- McGregor, S., Timmermann, A., & Timm, O. (2010). A unified proxy for ENSO and PDO variability since 1650. *Climate of the Past*, 5(5), 2177–2222. <https://doi.org/10.5194/cpd-5-2177-2009>
- Meehl, G. A., & Teng, H. (2007). Multi-model changes in El Niño teleconnections over North America in a future warmer climate. *Climate Dynamics*, 29(7–8), 779–790. <https://doi.org/10.1007/s00382-007-0268-3>
- Power, S., Delage, F., Chung, C., Kociuba, G., & Keay, K. (2013). Robust twenty-first-century projections of El Niño and related precipitation variability. *Nature*, 502(7472), 541–545. <https://doi.org/10.1038/nature12580>
- Power, S. B., Delage, F., Colman, R., & Moise, A. (2012). Consensus on twenty-first-century rainfall projections in climate models more widespread than previously thought. *Journal of Climate*, 25(11), 3792–3809. <https://doi.org/10.1175/JCLI-D-11-00354.1>
- Stevenson, S., Fox-Kemper, B., Jochum, M., Neale, R., Deser, C., & Meehl, G. (2012). Will there be a significant change to el Niño in the twenty-first century? *Journal of Climate*, 25(6), 2129–2145. <https://doi.org/10.1175/JCLI-D-11-00252.1>
- Stevenson, S. L. (2012). Significant changes to ENSO strength and impacts in the twenty-first century: Results from CMIP5. *Geophysical Research Letters*, 39, L17703. <https://doi.org/10.1029/2012GL052759>
- Taschetto, A. S., Sen Gupta, A., Jourdain, N. C., Santoso, A., Ummenhofer, C. C., & England, M. H. (2014). Cold tongue and warm pool ENSO events in CMIP5: Mean state and future projections. *Journal of Climate*, 27(8), 2861–2885. <https://doi.org/10.1175/JCLI-D-13-00437.1>
- Taylor, K. E., Stouffer, R. J., & Meehl, G. A. (2012). An overview of CMIP5 and the experiment design. *Bulletin of the American Meteorological Society*, 93(4), 485–498. <https://doi.org/10.1175/BAMS-D-11-00094.1>
- Trenberth, K. E., Branstator, G. W., Karoly, D., Kumar, A., Lau, N. C., & Ropelewski, C. (1998). Progress during TOGA in understanding and modeling global teleconnections associated with tropical sea surface temperatures. *Journal of Geophysical Research*, 103, 14,291–14,324. <https://doi.org/10.1029/97JC01444>
- Watanabe, M., Kamae, Y., & Kimoto, M. (2014). Robust increase of the equatorial Pacific rainfall and its variability in a warmed climate. *Geophysical Research Letters*, 41, 3227–3232. <https://doi.org/10.1002/2014GL059692>
- Watanabe, M., Kug, J.-S., Jin, F.-F., Collins, M., Ohba, M., & Wittenberg, A. T. (2012). Uncertainty in the ENSO amplitude change from the past to the future. *Geophysical Research Letters*, 39, L20703. [https://doi.org/10.1029/2012GL053305\(20\)](https://doi.org/10.1029/2012GL053305(20))
- Weare, B. C. (2013). El Niño teleconnections in CMIP5 models. *Climate Dynamics*, 41(7–8), 2165–2177. <https://doi.org/10.1007/s00382-012-1537-3>
- Wittenberg, A. T. (2009). Are historical records sufficient to constrain ENSO simulations? *Geophysical Research Letters*, 36, L12702. <https://doi.org/10.1029/2009GL038710>
- Xie, P. P., & Arkin, P. A. (1997). Global precipitation: A {17-year} monthly analysis based on gauge observations, satellite estimates, and numerical model outputs. *Bulletin of the American Meteorological Society*, 78(11), 2539–2558. [https://doi.org/10.1175/1520-0477\(1997\)078%3C2539:GPAYMA%3E2.0.CO;2](https://doi.org/10.1175/1520-0477(1997)078%3C2539:GPAYMA%3E2.0.CO;2)
- Zhou, Z. Q., Xie, S. P., Zheng, X. T., Liu, Q., & Wang, H. (2014). Global warming-induced changes in El Niño teleconnections over the North Pacific and North America. *Journal of Climate*, 27(24), 9050–9064. <https://doi.org/10.1175/JCLI-D-14-00254.1>